

Supplementary information

Synergistic Oxygen Reduction of Dual Redox Catalysts Boosting the Power of Lithium-Air Battery

Yun Guang Zhu, F. W. Thomas Goh, Ruiting Yan, Sisi Wu, Stefan Adams, Qing Wang*

Department of Materials Science and Engineering, Faculty of Engineering, National University of Singapore, Singapore 117576

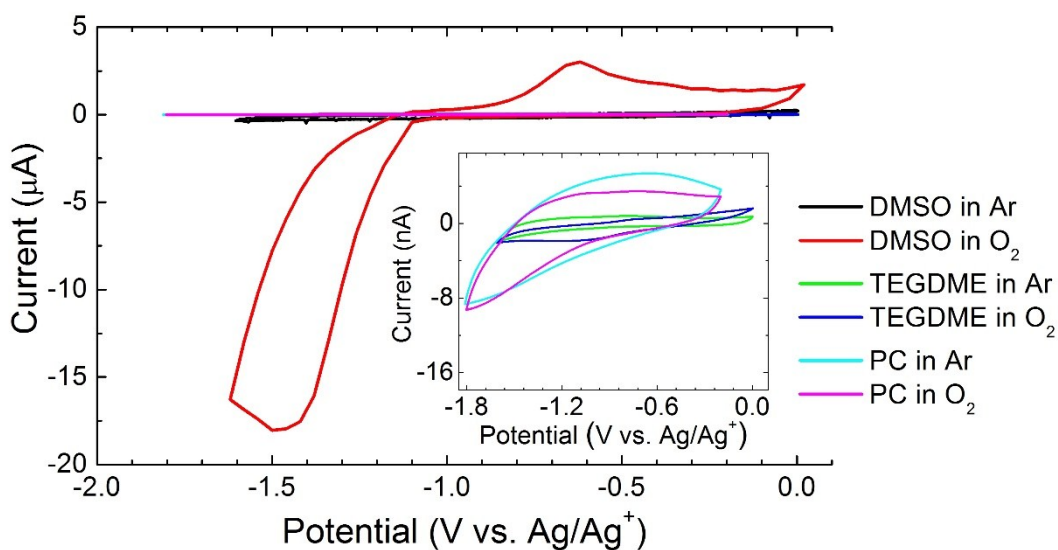


Fig. S1. CV curves of three different electrolytes with 0.1 M LiTFSI dissolved in DMSO, TEGDME, or PC saturated with Ar or O₂. The working electrode is a Pt disk. The scan rate is 0.1 V·s⁻¹.

Discussion of Fig. S1: According to the oxygen reduction and oxidation current densities, oxygen in DMSO shows highest activity among the three solvents. Therefore, DMSO is selected as the studied solvent in this work pursuing high power densities of redox flow lithium-air batteries.

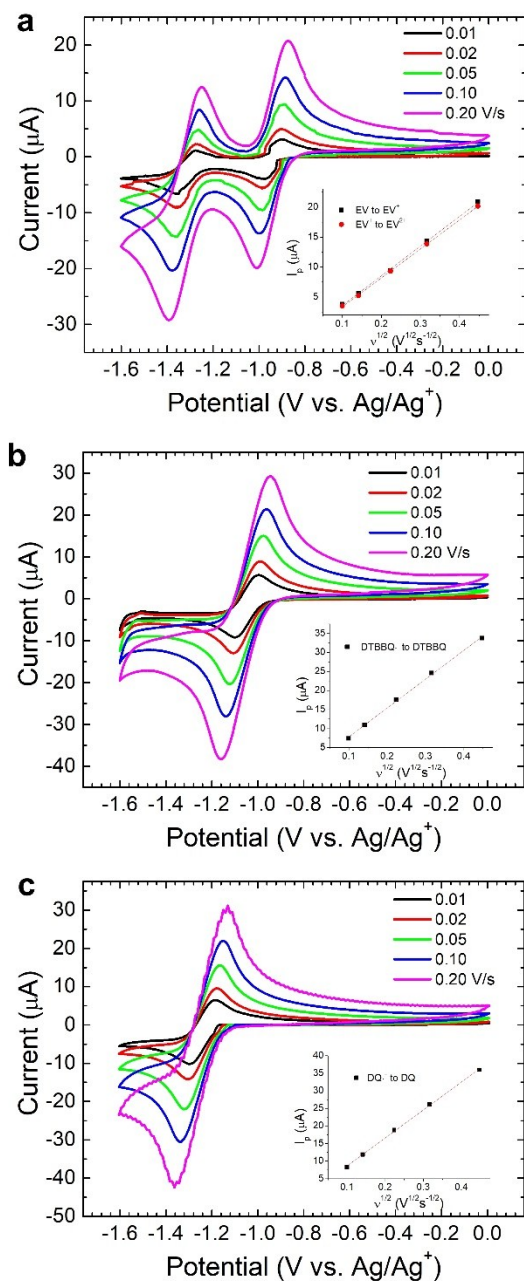


Fig. S2. CV curves of 10 mM EV (a), DTBBQ (b), and DQ (c) in 0.1 M LiTFSI/DMSO in Ar atmosphere. The insets in each figure show the relationship between scan rates ($v^{1/2}$) and peak currents (i_p).

Discussion of Fig. S2: According to the CV measurements under different scan rates, all three redox mediators show diffusion-limited reversible electrochemical redox reactions. The diffusion coefficients of them are calculated based on ultra-microelectrode (UME) measurements, as shown in Table S1.

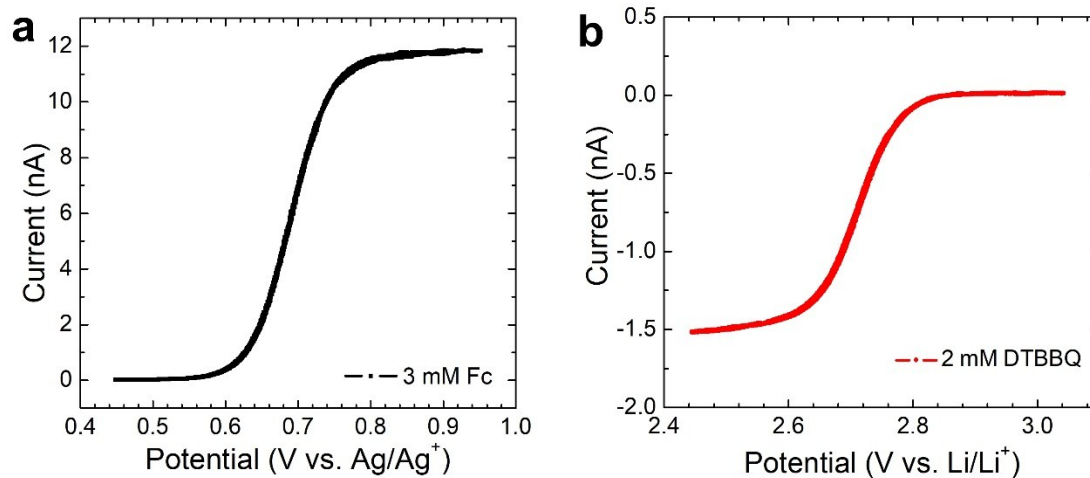


Fig. S3. (a) CV curve of 3 mM Fc in 0.5M TBABF₄/ACN for calibration of UME. (b) CV curve of 2 mM DTBBQ in 0.1 M LiTFSI/DMSO electrolyte by using the aforementioned UME. The reference electrode is Ag wire. For the CV curve of DTBBQ, the potential of Ag wire was calibrated by using standard Ag/Ag⁺. The scan rate was 0.01 V·s⁻¹. The potential of Ag/Ag⁺ is 3.90 V vs. Li/Li⁺ in DMSO-based electrolyte.

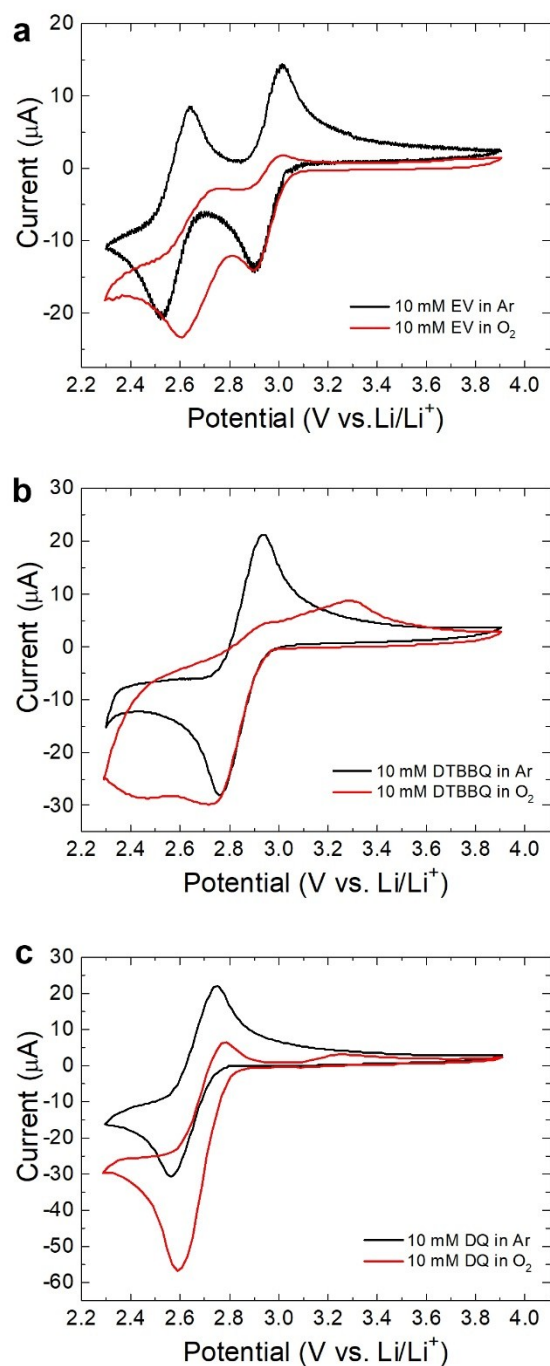


Fig. S4. CV curves of three redox molecules (a) EV, (b) DTBBQ and (c) DQ in 0.1 M LiTFSI/DMSO saturated with Ar or O₂. The scan rate was 0.1 V·s⁻¹. The potential of Ag/Ag⁺ is 3.90 V vs. Li/Li⁺ in DMSO-based electrolyte.

Discussion of Fig. S4: According to the CV measurements in saturated Ar and O₂ electrolytes, it is worth noting that both DTBBQ and DQ electrolytes exhibits a small oxidation peak at ~0.65 V vs. Ag/Ag⁺, which should be attributed to oxidation of superoxide species. As a control experiment, viologen electrolyte doesn't show such oxidation peak. Therefore, we assume that quinone species can enhance the lifetime of superoxide species, which is assumed the formation of Li-quinone-O₂⁻ complex.

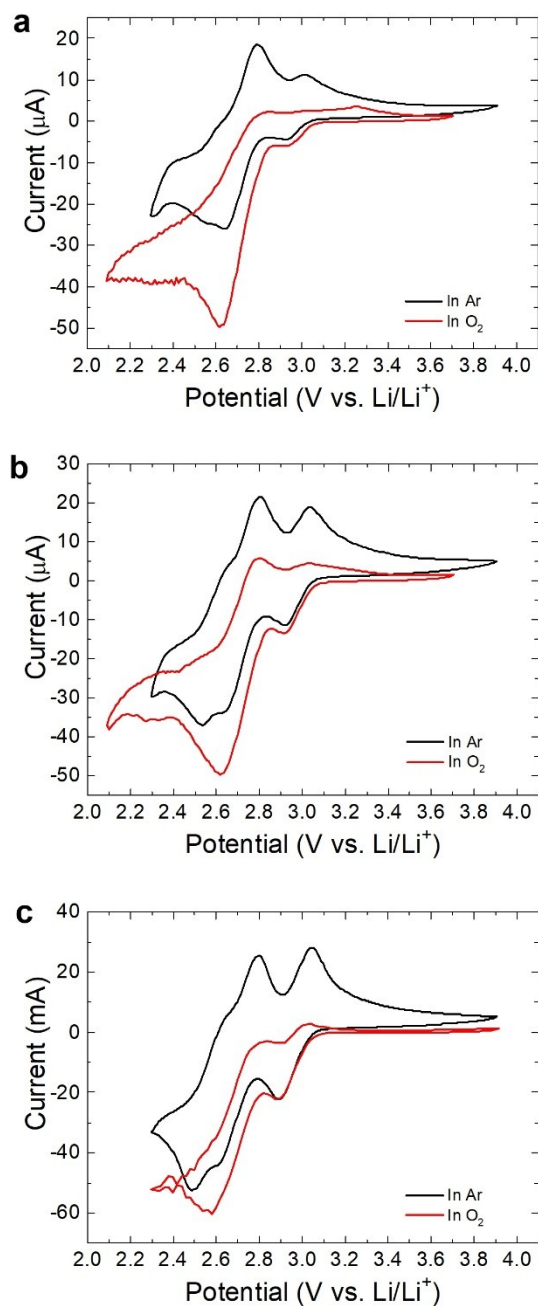


Fig. S5. CV curves of EV-DQ with different concentrations of (a) 2 mM/10 mM, (b) 5 mM/10 mM, (c) 10 mM/10 mM in 0.1 M LiTFSI/DMSO saturated with Ar or O₂. The scan rate is 0.1 V·s⁻¹. The potential of Ag/Ag⁺ is 3.90 V vs. Li/Li⁺ in DMSO-based electrolyte.

Discussion of Fig. S5: Although Li-quinone-O₂⁻ species shows less reactive than radical O₂⁻, it still causes directed reduction on cathode in redox flow lithium-oxygen battery (RFLOB), causing passivation and clogging. Therefore, we utilize EV to shorten the lifetime of Li-quinone-O₂⁻ species and stabilize the cathode.

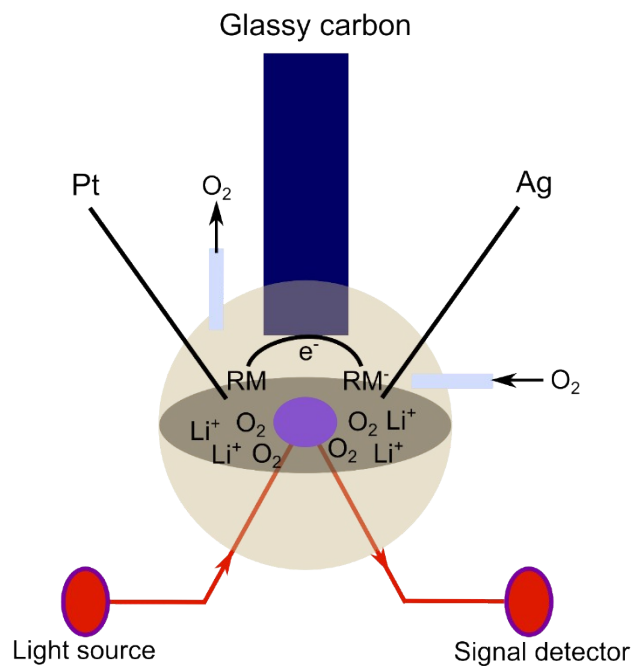


Fig. S6. Schematic of the *in-situ* spectroelectrochemical FTIR cell. It consists of an optical window (purple area), oxygen inlet and outlet, a glassy carbon working electrode, a Pt counter electrode, and a Ag wire reference electrode. Prior to the test, the electrolyte is bubbled with argon or oxygen gas for half an hour.

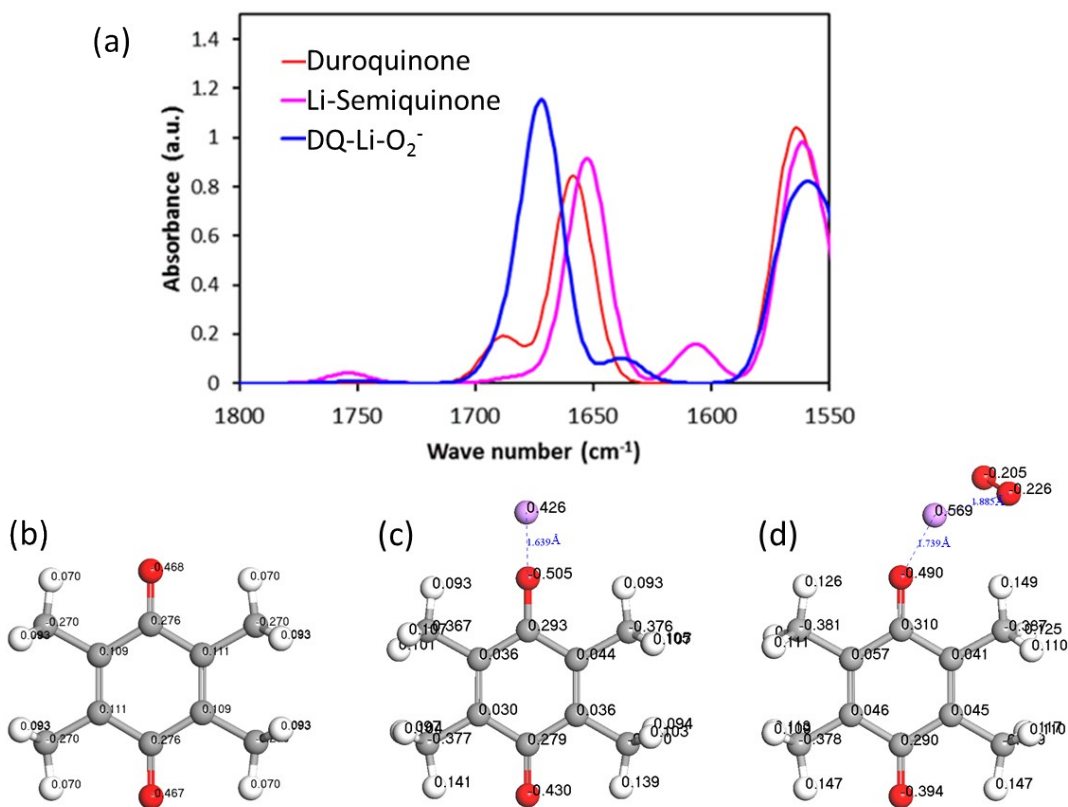


Fig. S7. (a) Calculated IR absorbance of duroquinone at three different states in the presence of oxygen and Li⁺: (b-d) Mulliken charges of atoms in (b) duroquinone, (c) the corresponding lithium semiquinone and (d) the duroquinone lithium superoxide formed by the interaction of the lithium semiquinone with molecular oxygen. While the effective charge of the isolated DQ is (trivially) zero, the semiquinone radical anion in (c) has an effective charge of -0.43e, and the partially re-oxidized DQ component of the superoxide complex in (d) retains a charge of -0.14e only, while the oxygen molecule is reduced to the superoxide with an effective charge of -0.43e. In line with the reduced Coulombic attraction the equilibrium Li-O distance increases from 1.64 Å in the semiquinone to 1.74 Å in the DQ-Li-O₂⁻ superoxide complex anion.

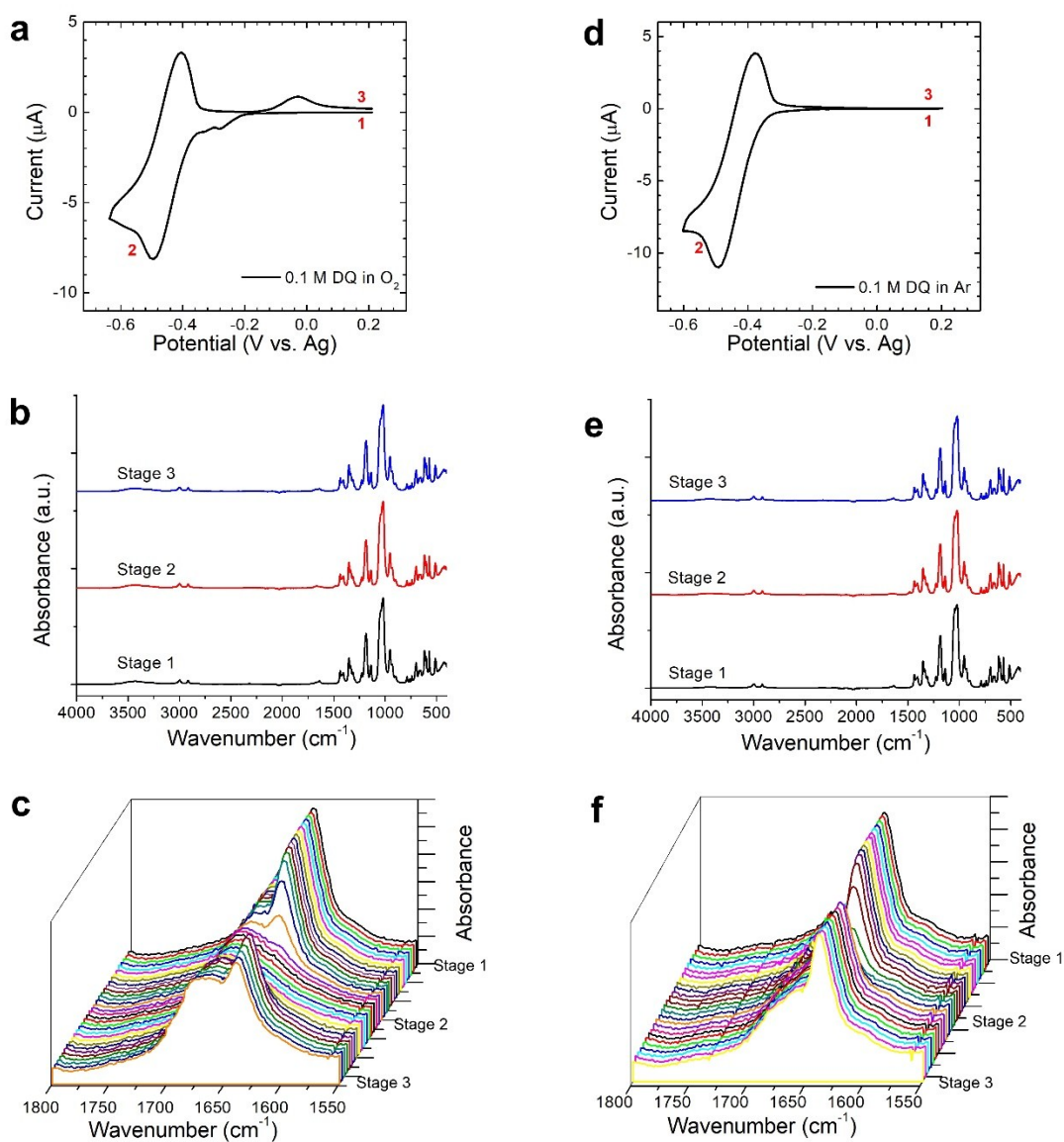


Fig. S8. *In-situ* electrochemical FTIR spectra of 100 mM DQ in 1 M LiTFSI/DMSO with saturated O₂ and Ar. (a) shows the CV curve of DQ with saturated O₂; (b) shows the FTIR spectra collected at three different stages of CV measurement; (c) The spectra highlighted in the wavenumber range from 1800 to 1550 cm⁻¹. (d, e, and f) shows the corresponding CV curve and FTIR spectra of the DQ electrolyte in Ar. The scan rate is 0.1 V·s⁻¹ in the CV measurements.

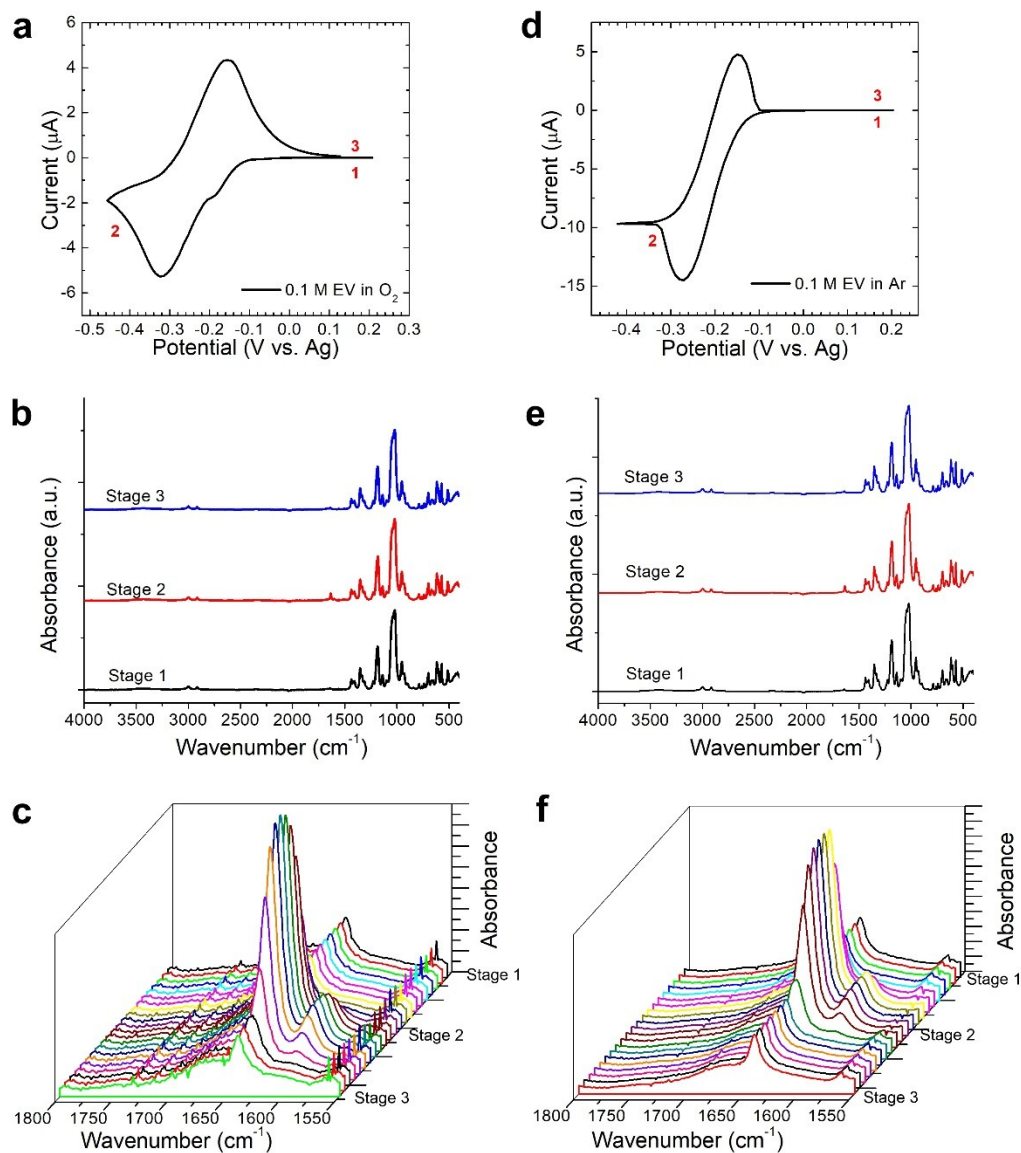


Fig. S9. *In-situ* electrochemical FTIR spectra of 100 mM EV in 1 M LiTFSI/DMSO with saturated O₂ and Ar. (a) shows the CV curve of EV with saturated O₂; (b) shows the FTIR spectra collected at three different stages of CV measurement; (c) The spectra highlighted in the wavenumber range from 1800 to 1550 cm⁻¹. (d, e, and f) shows the corresponding CV curve and FTIR spectra of the EV electrolyte in Ar. The scan rate is 0.1 V·s⁻¹ in the CV measurements.

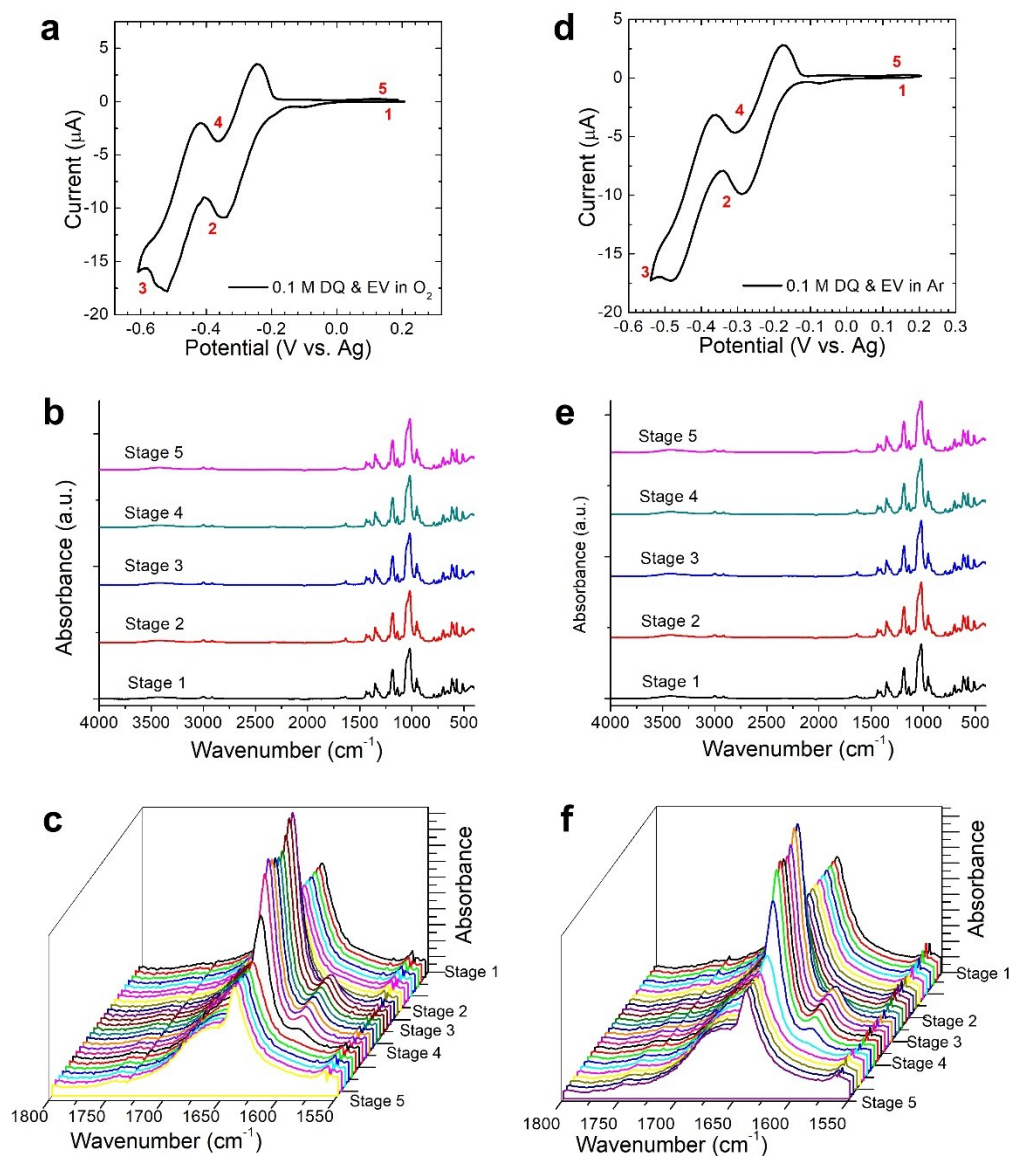


Fig. S10. *In-situ* electrochemical FTIR spectra of EV-DQ (100/100 mM) in 1 M LiTFSI/DMSO with saturated O_2 and Ar. (a) shows the CV curve of EV-DQ with saturated O_2 ; (b) shows the FTIR spectra collected at five different stages of CV measurement; (c) The spectra highlighted in the wavenumber range from 1800 to 1550 cm^{-1} . (d, e, and f) shows the corresponding CV curve and FTIR spectra of the EV-DQ electrolyte in Ar. The scan rate is $0.1 V \cdot s^{-1}$ in the CV measurements.

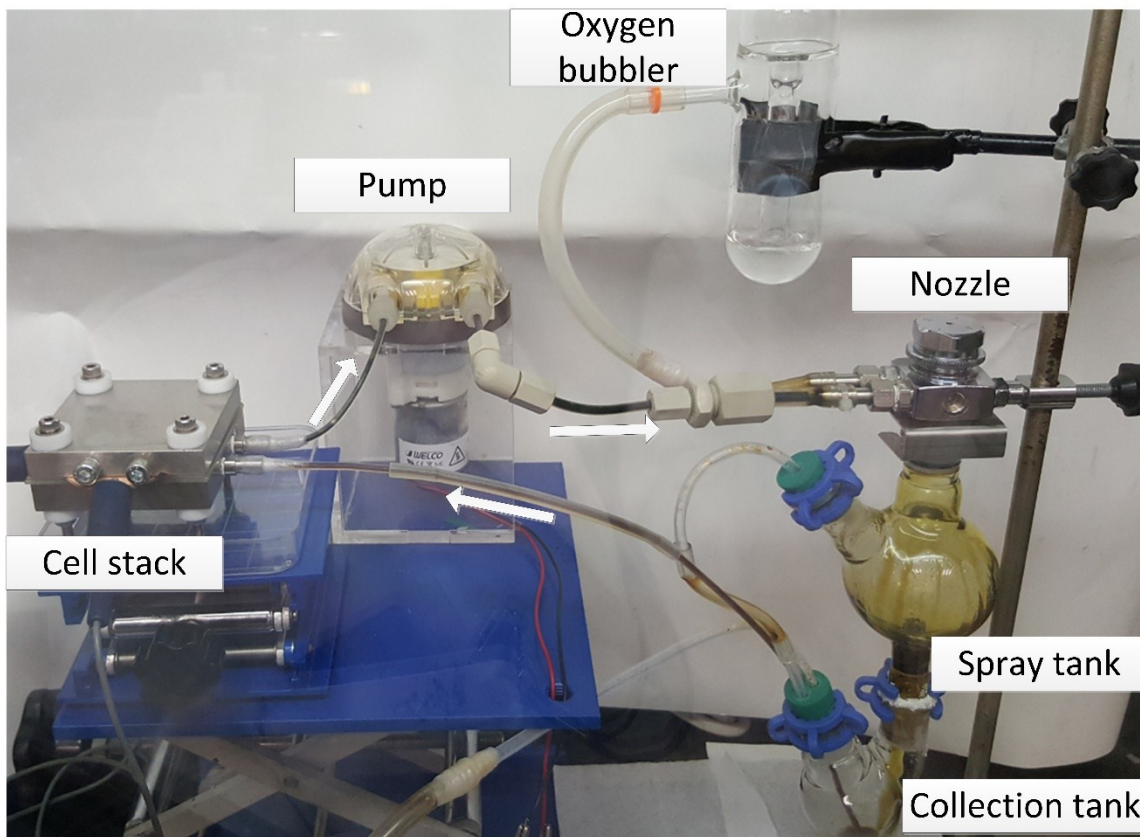


Fig. S11. Photograph of the Li fuel cell setup. It consists of a cell stack, spray tank (gas diffusion tank), electrolyte collection tank, peristaltic pump, oxygen bubbler, and nozzle.

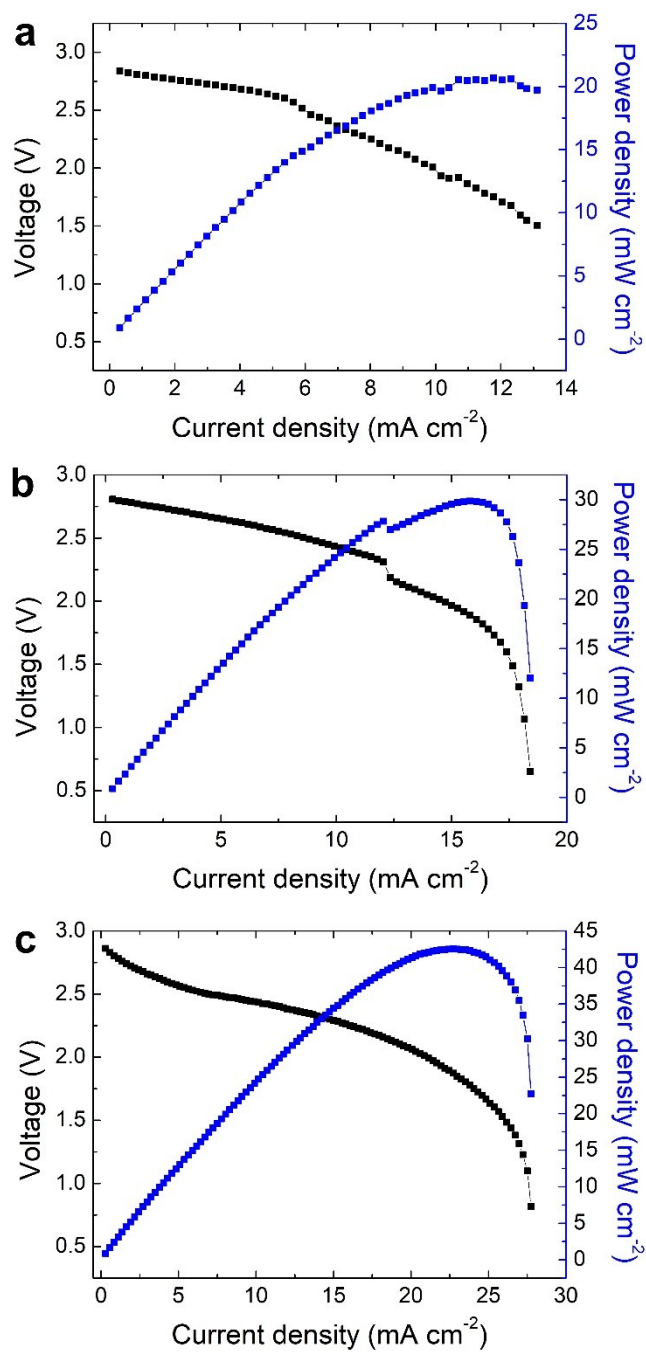


Fig. S12. Voltage (black) and power density (blue) versus current density for Li fuel cell in the presence of 50 mM EV (a), DTBBQ (b), and DQ (c) in 1 M LiTFSI/DMSO electrolyte under O_2 spray.

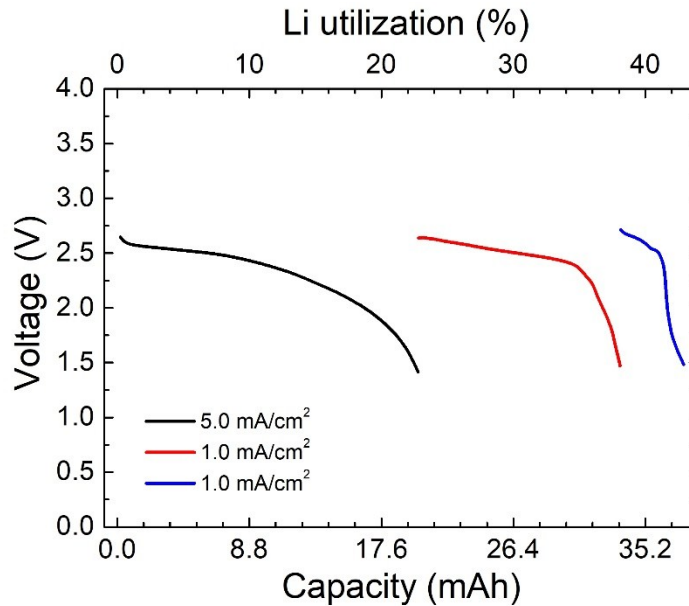


Fig. S13. Discharge voltage profiles for 100 mM DQ in 1 M LiTFSI/DMSO under O₂ spray. The cell was relaxed and discharged at a lower current density when the voltage went down to the cut-off voltage 1.40 V.

Discussion of Fig. S13: As shown in the discharge profile of DQ electrolyte, the discharge voltage dropped very fast after ~7 mAh under current density of 5.0 mA/cm², which can be attributed to the passivation of electrolyte by discharge products from direct reduction of Li-DQ-O₂⁻ complex. Even under low current density of 1.0 mA/cm² after ~1 h rest, the discharge capacity cannot be extended too much. The total utilization of Li metal after three times discharge was only around 43 %, which cannot guarantee high energy density of RFLOB.

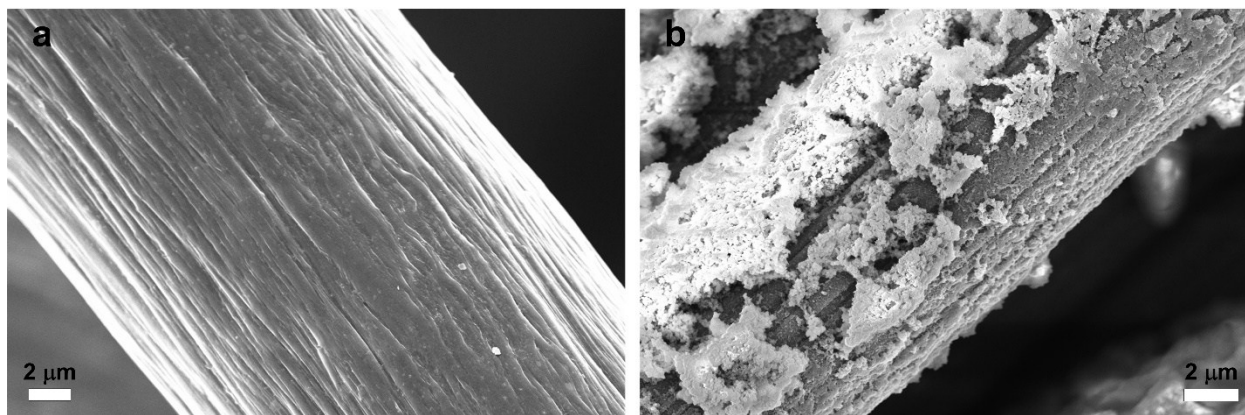


Fig. S14. Morphologies of carbon felt in cathode before (a) and after (b) ~37 mAh of discharge. The electrolyte was 100 mM DQ in 1 M LiTFSI/DSMO under O₂ spray.

Discussion of Fig. S14: As shown in the SEM image of carbon felt in cathode before and after discharge process, the passivation of cathode was serious, which should be from the direct reduction of Li-DQ-O₂⁻ complex.

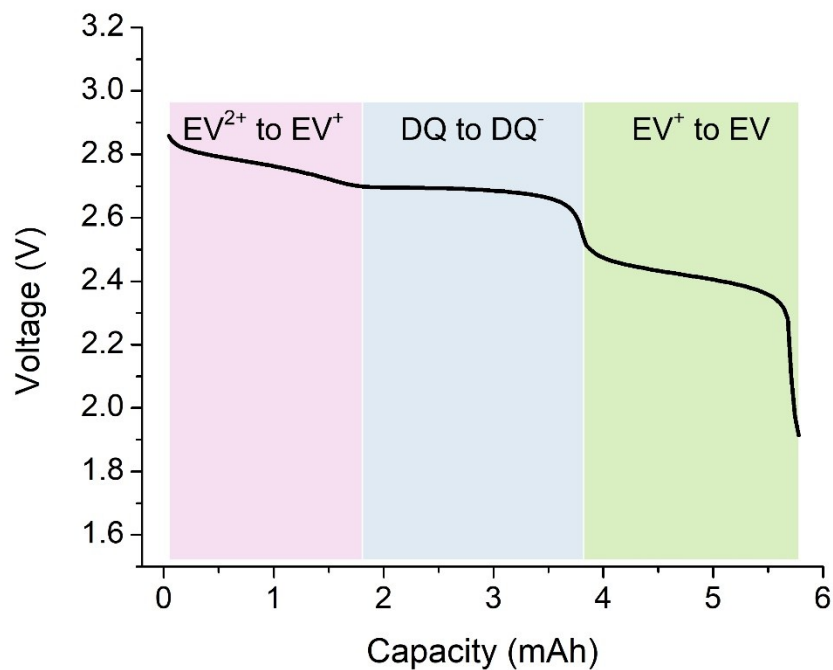


Fig. S15. Discharge voltage profiles for 3 mL 20 mM DQ & 20 mM EV in 1 M LiTFSI/DMSO in an Ar-filled glove box. The cell was discharged at $2 \text{ mA} \cdot \text{cm}^{-2}$ to a cut-off voltage 2.0 V. The three plateaus exhibit the reduction process of the two redox mediators. The electron-transfer number is slightly more than 1, which may be attributed to some side reactions.

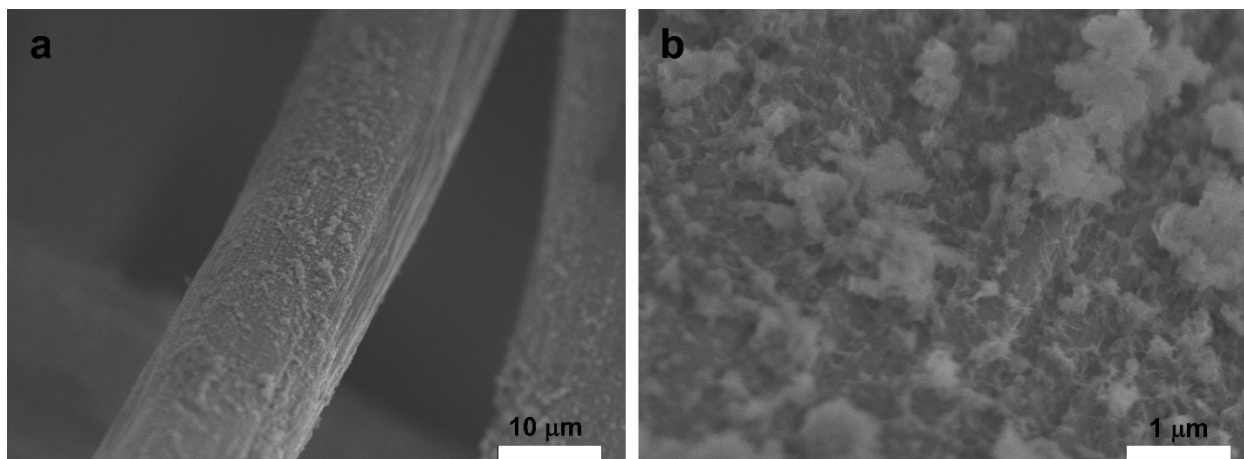


Fig. S16. Morphologies of carbon felt in cathode after ~80 mAh of discharge capacity under O₂ spray. The electrolyte was EV-DQ (0.2 M/0.2 M) in 1 M LiTFSI/DSMO.

Discussion of Fig. S16. As shown in the SEM images of carbon felt in cathode after ~80 mAh of discharge capacity, the surface was covered with much less discharge products than the cell with DQ electrolyte (Fig S14). Through the comparison, it is further confirmed that EV can be used to shorten the lifetime of Li-DQ-O₂⁻ and enhance the stability of cathode.

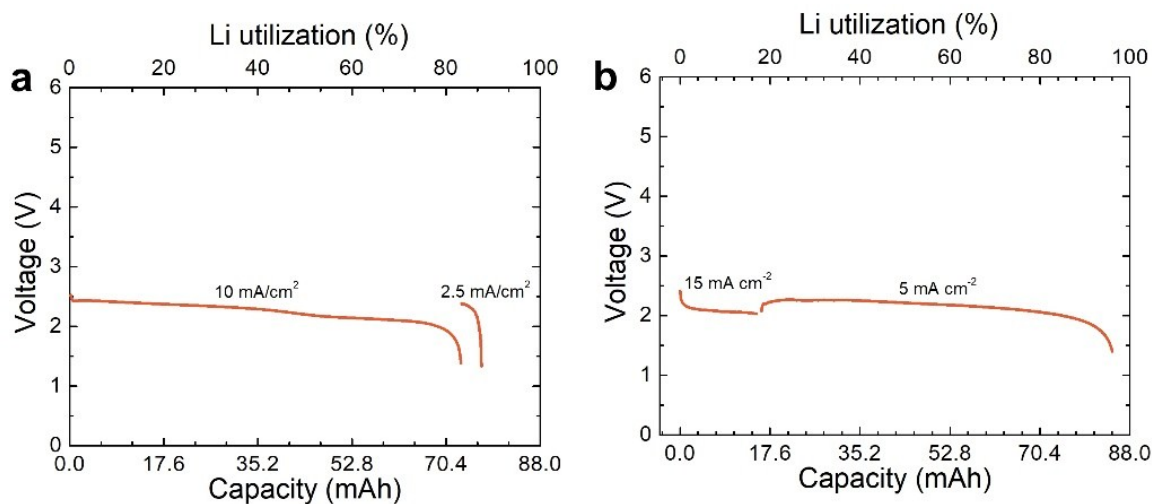


Fig. S17. Discharge curves of RFLOB under high current densities in the presence of (a) EV-DQ (0.1 M/0.2 M) and (b) EV-DQ (0.2 M/0.1 M) under O_2 spray. The electrolyte was 1 M LiTFSI/DSMO.

Discussion of Fig. S17: The RFLOBs with different ratio of EV/DQ electrolytes was evaluated through galvanic discharge test, as shown in Fig. S17. It shows that the RFLOB with high ratio of EV/DQ (2/1) exhibited a better utilization of lithium metal (~96 %). We believe the intermediate ($Li-DQ-O_2^-$) can cross over to anode side causing parasitic reaction with Li and lower its utilization.

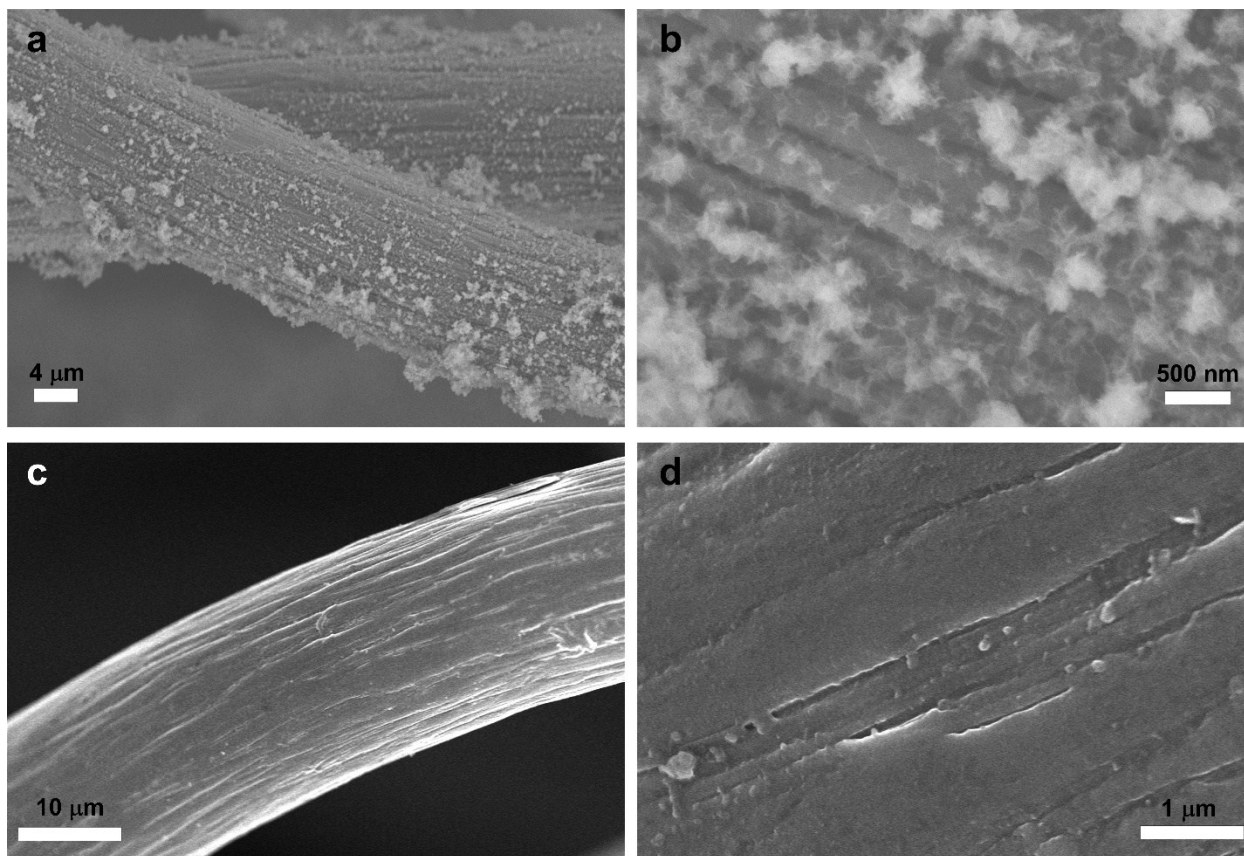


Fig. S18. Morphologies of carbon felts in cathode after ~ 80 mAh of discharge under O_2 spray with EV-DQ (0.1/0.2 M, a and b) and EV-DQ (0.2/0.1 M, c and d) in 1 M LiTFSI/DSMO. The cathode with the high ratio of EV-DQ (0.2/0.1 M) exhibits much cleaner surface after fully discharge of RFLOB.

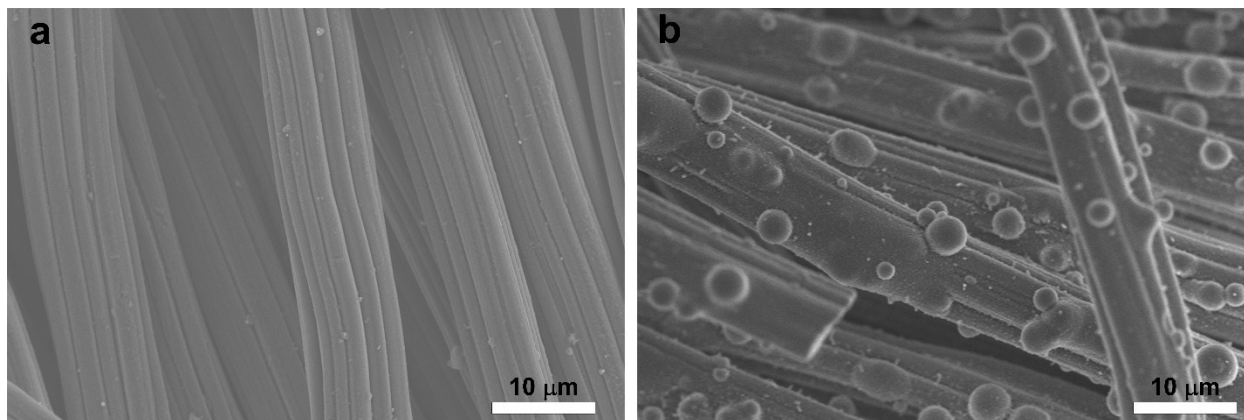


Fig. S19. Morphologies of carbon cloth in the gas diffusion tank as filter before (a) and after (b) ~80 mAh of discharge under O₂ spray. The electrolyte was EV-DQ (0.2 M /0.2 M) in 1 M LiTFSI/DSMO.

Discussion of Fig. S19: According to the working principle of RFLOB, most of oxygen reduction products should be collected in the tank. We used carbon cloth as a filter to collect oxygen reduction products. After carefully rinsing the carbon cloth by acetonitrile, we dried it at room temperature under vacuum condition for SEM measurements. As shown in Figure S19b, the surface of carbon cloth was covered by lots of micro sphere particles, which was characterized by FTIR (Fig S20) as the mixture of Li₂O₂/Li₂CO₃.

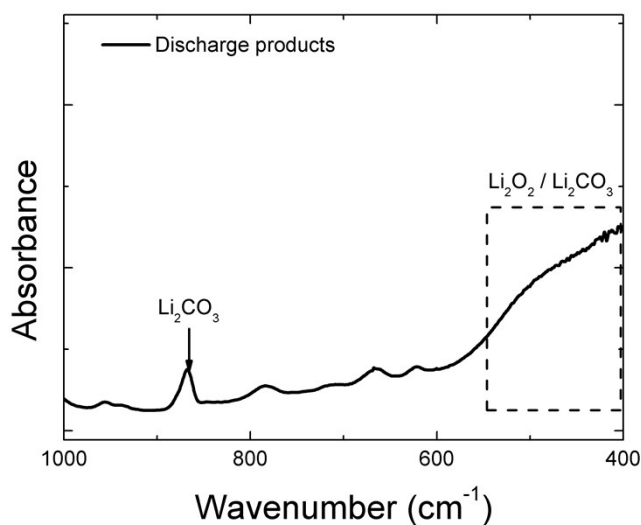


Fig. S20. The FTIR spectrum of the discharge products on carbon cloth in GDT after ~80 mAh of discharge with EV-DQ (0.2 M/0.2 M) electrolyte.

Table S1. Electrochemical parameters of different RMs measured in 0.1 M LiTFSI/DMSO.

Solution	Concentration (mM)	$E_{1/2}$ of the 1 st reaction (V vs. Li/Li ⁺)	i_{ss} of the 1 st peak (nA)	$E_{1/2}$ of the 2 nd reaction (V vs. Li/Li ⁺)	i_{ss} of the 2 nd peak (nA)	D_0 for the 1 st reduction (cm ² ·s ⁻¹)	D_0 for the 2 nd reduction (cm ² ·s ⁻¹)
DTTBQ	2	2.71	1.5	-	-	3.3×10^{-6}	-
DQ	2	2.66	1.75	-	-	3.8×10^{-6}	-
EV	2	2.88	1.06	2.51	1.19	2.3×10^{-6}	2.6×10^{-6}
Fc standard	3	-	11.7	-	-	1.7×10^{-5}	-

According to **equation (1)**, the diffusion coefficients of the three RMs in DMSO-based electrolyte were obtained as listed in **Table S1**.

$$i_{ss} = 4nFD_0C_0r_0 \quad (1)$$

Where i_{ss} is the steady-state current (A); n is the electron transfer number of the redox reaction; D_0 is the diffusion coefficient of the redox molecule (cm²·s⁻¹); C_0 is the concentration of redox molecule in the bulk electrolyte (mol·cm⁻³); r_0 is the radius of UME (cm), calibrated by using a standard reference electrolyte (3 mM Fc in 0.5M TBABF₄/ACN), in which the diffusion coefficient was reported as 1.7×10^{-5} cm²·s⁻¹.¹

Table S2. Power densities for reported Li-O₂ battery systems and the comparison with RFLOB system reported here.

Systems	Average voltage (V)	Current density (mA·cm ⁻²)	Power density (mW·cm ⁻²)
Li-O ₂ battery with molten salts ¹	2.75	0.64	1.76
Li-O ₂ battery with TiC as a solid electrocatalyst ²	2.50	2.50	6.25
Li-O ₂ battery with RuO ₂ as a solid electrocatalyst ³	2.75	0.50	1.33
Li-O ₂ battery with DTBBQ as a soluble catalyst ⁴	2.60	2.00	5.20
Li-O ₂ battery with FePc as a soluble catalyst ⁵	2.69	0.30	0.81
RFLOB with EV as a soluble catalyst ⁶	2.70	0.125	0.34
Primary static Li-O ₂ battery ⁷	2.20	0.50	1.10
RFLOB with dry air spray (this work)	2.20	10.0	22.0
RFLOB with O ₂ spray (this work)	2.40	15.0	36.0

Reference

1. Giordani, V.; Tozier, D.; Tan, H.; Burke, C. M.; Gallant, B. M.; Uddin, J.; Greer, J. R.; McCloskey, B. D.; Chase, G. V.; Addison, D., *Journal of the American Chemical Society* 2016, 138 (8), 2656-2663.
2. Ottakam Thotiyl, M. M.; Freunberger, S. A.; Peng, Z.; Chen, Y.; Liu, Z.; Bruce, P. G., *Nature Materials* 2013, 12 (11), 1050-1056.
3. Li, F.; Tang, D. M.; Zhang, T.; Liao, K.; He, P.; Golberg, D.; Yamada, A.; Zhou, H., *Advanced Energy Materials* 2015, 5 (13), 1500294.
4. Gao, X.; Chen, Y.; Johnson, L. R.; Jovanov, Z. P.; Bruce, P. G., *Nature Energy* 2017, 2, 17118.
5. Sun, D.; Shen, Y.; Zhang, W.; Yu, L.; Yi, Z.; Yin, W.; Wang, D.; Huang, Y.; Wang, J.; Wang, D., *Journal of the American Chemical Society* 2014, 136 (25), 8941-8946.
6. Zhu, Y. G.; Jia, C.; Yang, J.; Pan, F.; Huang, Q.; Wang, Q., *Chemical Communications* 2015, 51 (46), 9451-9454.
7. Zhang, S. S.; Read, J., *Journal of Power Sources* 2011, 196 (5), 2867-2870.